Jefferson Lab PAC 32 Letter of Intent

The Longitudinal Photon, Transverse Nucleon, Single-Spin Asymmetry in Exclusive Pion Electroproduction

D. Dutta,[1] D. Gaskell,[2] and G.M. Huber[3]

[1] *Mississippi State University, Mississippi State, MS 39762 USA*

[2] *Jefferson Lab, Newport News, VA 23606 USA*

[3] *University of Regina, Regina, SK S4S-0A2 Canada*

(Dated: June 15, 2007)

Abstract

We intend to measure the transverse single-spin asymmetry in the exclusive pion production $n(e,e'\vec{p})\pi^-$ reaction, using a ^{2}H target. This polarization variable has been noted as being especially sensitive to the spin-flip generalized parton distribution (GPD) $\tilde{E}$, and factorization studies have indicated that precocious scaling is likely to set in at moderate $Q^2 \sim 2-4$ GeV^2, as opposed to the absolute cross section, where scaling is not expected until $Q^2 \geq 10$ GeV^2. Furthermore, this variable has been noted as being important for the reliable extraction of the charged pion form factor from pion electroproduction. We intend to pursue this study using the SHMS–HMS spectrometer combination in Hall C, with the hadron arm equipped with the focal plane polarimeter (FPP). The recoil polarization technique is proposed to be used instead of a transversely polarized target, so that significantly higher luminosities can be used, reducing the total beamtime requirement. **A crucial aspect of our experiment is the Rosenbluth L/T separation.** Unlike other ongoing or proposed experiments, where the dominance of the longitudinal contribution to the spin asymmetry at intermediate Q^2 is simply assumed, we intend to demonstrate whether this is in fact the case. This is important, because factorization has only been proven for the case of longitudinal photons. Data from this experiment will thus indicate whether the precocious scaling expectations of the GPD formalism will be ultimately realized, as well as helping to constrain longitudinal backgrounds possibly complicating the extraction of the pion form factor from electroproduction experiment data.

I. CONTRIBUTION TO THE HALL C 12 GEV UPGRADE

Dipangkar Dutta will....

David Gaskell will support the SHMS construction and detector assembly as part of his general Hall C support duties. In addition, he will devote a significant fraction of his "Research" time to work on the Hall C upgrade. In particular, he will devote time to updating and maintaining the Hall C simulation package SIMC. This will entail, not only incorporating the SHMS into the existing simulation, but helping with spectrometer optics calculations to guide the design and construction of the SHMS.

Garth Huber intends to apply to the Natural Sciences and Engineering Research Council of Canada (NSERC) for a Research Tools and Instrumentation grant (approximately $100kUSD) in support of the SHMS Heavy Gas Čerenkov detector. Given the currently-projected CD2 and CD3 review schedule, this application will likely be submitted in October, 2008. Should these funds be granted by the Government of Canada, he intends to lead the construction efforts of this detector in collaboration with Hall C scientific and technical staff. In either event, the Regina group intends to provide manpower in support of the R&D, construction and commissioning of this detector.

II. SCIENTIFIC JUSTIFICATION

A. Generalized Parton Distributions and Contribution from the Pion Pole

In recent years, much progress has been made in the theory of generalized parton distributions (GPDs). Unifying the concepts of parton distributions and of hadronic form factors, they contain a wealth of information about how quarks and gluons make up hadrons. The key difference between the usual parton distributions and their generalized counterparts can be seen by representing them in terms of the quark and gluon wavefunctions of the hadron. While the usual parton distributions are obtained from the squared hadron wavefunction representing the probability to find a parton with specified polarization and longitudinal momentum fraction x in the fast moving hadron (Fig. 1a), GPDs represent the interference of different wavefunctions, one where the parton has momentum fraction $x + \xi$ and one where this fraction is $x - \xi$ (Fig. 1b). GPDs thus correlate different parton configurations in the hadron at the quantum mechanical level. A special kinematic regime is probed in deep exclusive meson production, where the initial hadron emits a quark-antiquark or gluon pair (Fig. 1c). This has no counterpart in the usual parton distributions and carries information about $q\bar{q}$ and gg-components in the hadron wavefunction.

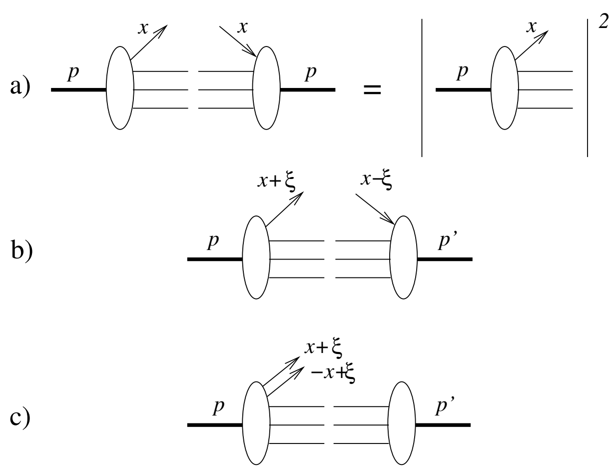

FIG. 1: (a) Usual parton distribution, representing the probability to find a parton with momentum fraction x in the nucleon. (b) GPD in the region where it represents the emission of a parton with momentum fraction $x + \xi$ and its reabsorption with momentum fraction $x - \xi$. (c) GPD in the region where it represents the emission of a quark-antiquark pair, and has no counterpart in the usual parton distributions. This figure has been adapted from Ref. [1].

Apart from the momentum fraction variables x and ξ, GPDs depend on the four momentum transfer t. This is an independent variable, because the momenta p and p' may differ in either their longitudinal or transverse components. GPDs thus interrelate the longitudinal and transverse momentum structure of partons within a fast moving hadron.

In order to access the physics contained within GPDs, one is restricted to the hard scattering regime. An important feature of hard scattering reactions is the possibility to separate clearly the perturbative and nonperturbative stages of the interaction. Qualitatively speaking, the presence of a hard probe allows one to create small size quark-antiquark and gluon configurations, whose interactions are described by perturbative QCD (pQCD). The nonperturbative stage of the reaction describes how the hadron reacts to this configuration, or how this probe is transformed into hadrons. This separation is the so-called factorization property of hard reactions. Hard exclusive meson electroproduction was first shown to be factorizable in Ref. [2]. This factorization applies when the virtual photon is longitudinally polarized, which corresponds to a small size configuration compared to a transversely polarized photon.

GPDs are universal quantities and reflect the structure of the nucleon independently of the reaction which probes the nucleon. At leading twist-2 level, the nucleon structure information can be parameterized in terms of four quark chirality conserving GPDs, denoted H, E, $\tilde{H}$ and $\tilde{E}$. H and E are summed over quark helicity, while $\tilde{H}$ and $\tilde{E}$ involve the difference between left and right handed quarks. H and $\tilde{H}$ conserve the helicity of the proton, while E and $\tilde{E}$ allow for the possibility that the proton helicity is flipped. Because quark helicity is conserved in the hard scattering regime, the produced meson acts as a helicity filter. In particular, leading order QCD predicts that vector meson production is sensitive only to the unpolarized GPDs, H and E, whereas pseudoscalar meson production is sensitive only to the polarized GPDs, $\tilde{H}$ and $\tilde{E}$. In contrast, deeply virtual compton scattering (DVCS) depends at the same time on both the polarized ($\tilde{H}$ and $\tilde{E}$) and the unpolarized (H and E) GPDs. This makes hard meson electroproduction reactions complementary to the DVCS process, as it provides an additional tool to disentangle the different GPDs [3].

Besides coinciding with the parton distributions at vanishing momentum transfer ξ, the GPDs have interesting links with other nucleon structure quantities. Their first moments are related to the elastic form factors of the nucleon through model-independent sum rules

[4]:

$$\sum_q e_q \int_{-1}^{+1} dx H^q(x,\xi,t) = F_1(t), \tag{1}$$

$$\sum_q e_q \int_{-1}^{+1} dx E^q(x,\xi,t) = F_2(t), \tag{2}$$

$$\sum_q e_q \int_{-1}^{+1} dx \tilde{H}^q(x,\xi,t) = G_A(t), \tag{3}$$

$$\sum_q e_q \int_{-1}^{+1} dx \tilde{E}^q(x,\xi,t) = G_P(t), \tag{4}$$

where e_q is the charge of the relevant quark, $F_1(t)$, $F_2(t)$ are the Dirac and Pauli elastic nucleon form factors, and $G_A(t)$, $G_P(t)$ are the isovector axial and pseudoscalar nucleon form factors. The t-dependence of $G_A(t)$ is poorly known, and although $G_P(t)$ is an important quantity, it remains highly uncertain because it is negligible at the momentum transfer of β-decay[5]. Because of PCAC, $G_P(t)$ alone receives contributions from $J^{PG} = 0^{--}$ states[6], which are the quantum numbers of the pion, and so $\tilde{E}$ contains an important pion pole contribution (Fig. 2a).

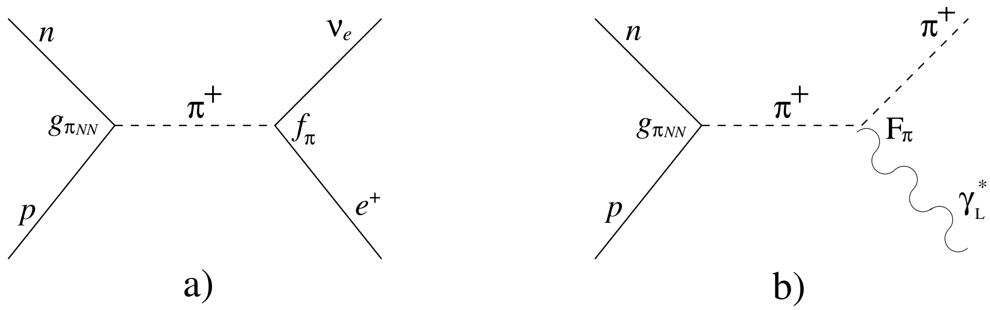

FIG. 2: (a) Pion pole contribution to $G_P(t)$, and hence to $\tilde{E}$. (b) Pion pole contribution to meson electroproduction at low $-t$.

Accordingly, Refs. [7, 8] have adopted the pion pole-dominated ansatz

$$\tilde{E}^{ud}(x,\xi,t) = F_\pi(t)\frac{\theta(\xi > |x|)}{2\xi}\phi_\pi(\frac{x+\xi}{2\xi}), \tag{5}$$

where $F_\pi(t)$ is the pion electromagnetic form factor, and ϕ_π is the pion distribution amplitude.

$\tilde{E}$ cannot be related to already known parton distributions, and so experimental information about $\tilde{E}$ via hard pion electroproduction can provide new information on nucleon structure which is unlikely to be available from any other source.

B. Single spin asymmetry in exclusive pion electroproduction

Frankfurt et al. [9] have considered a specific polarization observable which is the most sensitive observable to probe the spin-flip $\tilde{E}$. This variable is the single-spin asymmetry for exclusive charged pion production, using either a transversely polarized target or the equivalent recoil polarization measurement, and is defined [8] as

$$A_\perp = (\int_0^\pi d\beta \frac{d\sigma_L^\pi}{d\beta} - \int_\pi^{2\pi} d\beta \frac{d\sigma_L^\pi}{d\beta})(\int_0^{2\pi} d\beta \frac{d\sigma_L^\pi}{d\beta})^{-1}, \tag{6}$$

where $d\sigma_L^\pi$ is the exclusive charged pion electroproduction cross section using longitudinally polarized photons and β is the angle between the nucleon polarization vector and the reaction plane. Frankfurt et al. [9] have shown that this asymmetry must vanish if $\tilde{E}$ is zero. If $\tilde{E}$ is not zero, the asymmetry will display a sinβ dependence. Their predicted asymmetry using the $\tilde{E}$ ansatz from Ref. [10] is shown in Fig. 3.

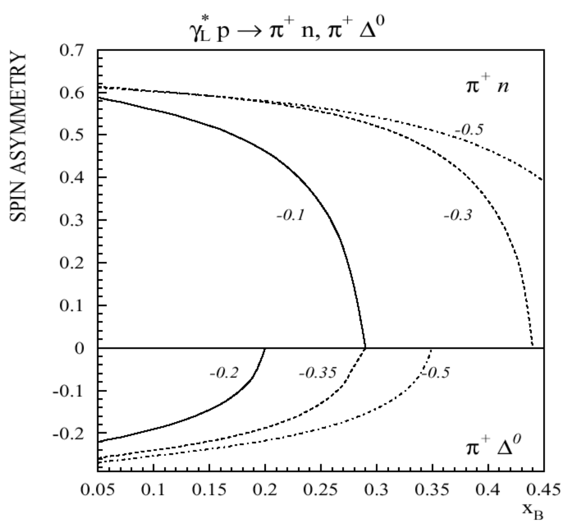

FIG. 3: Transverse single-spin asymmetry for the longitudinal electroproduction of $\pi^+ n$ and $\pi^+\Delta^0$ at different values of t [indicated on the curves in GeV^2] . The asymmetry drops to zero at the parallel kinematic limit, which is different for each t value, because the definition of P_y is ill-defined at this point. This figure is taken from Ref. [11].

Furthermore, it seems likely that a precocious factorization of the meson production amplitude into three parts – the overlap integral between the photon and pion wave functions, the hard interaction, and the GPD – will lead to a precocious scaling of $A_\perp$ as a function of Q^2 at moderate $Q^2 \sim 2-4$ GeV^2 [9]. This precocious scaling arises from the fact that higher order corrections, which may be significant at low Q^2, will likely cancel when one examines the ratio of two observables. In contrast, the onset of scaling for the absolute cross section is only expected for much larger values of $Q^2 \geq 10$ GeV^2.

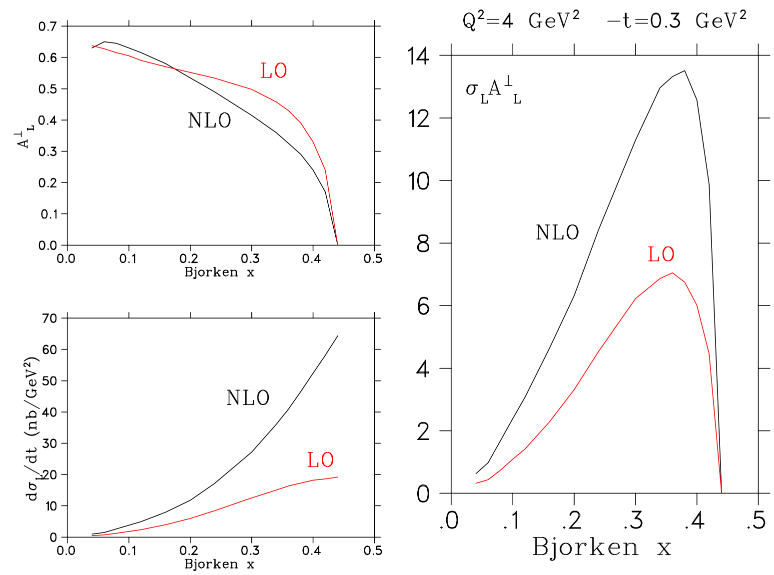

FIG. 4: Calculation of the transverse single-spin asymmetry including twist-four corrections by A. Belitsky [12] at $-t = 0.3$ GeV^2, $Q^2 = 4$ GeV^2. The red curves are the leading order calculation, while the black curves have twist-four power effects taken into account. While the cross section is very sensitive to these corrections, the transverse spin asymmetry is stable. The figure of merit $\sigma_L A_L^{\perp}$ maximum at $x = 0.37$ corresponds to particle angles and momenta which are similar to those proposed here.

This point is made clear in Fig. 4. This figure shows renormalon model calculations [12] of both the asymmetry and the longitudinal cross section at $Q^2 = 4$ GeV^2. While the magnitude of the cross section changes significantly when taking into account the twist-four corrections, the transverse spin asymmetry is essentially insensitive to them and displays the expected precocious scaling. The relatively low value of Q^2 for the expected onset of precocious scaling is important, because it will be experimentally accessible after the Jefferson Lab 12 GeV upgrade.

The well-known HERMES single-spin asymmetry result [13] in exclusive π^+ electroproduction was obtained for average values of $\langle x \rangle = 0.15$, $\langle Q^2 \rangle = 2.2$ GeV^2 and $\langle t \rangle = -0.46$ GeV^2. Using a hydrogen target polarized parallel to the incident electron beam, they observed an azimuthal polarization asymmetry and attributed this to the small target polarization component transverse to the reaction plane. This helped motivate their eventual installation of a target with polarization transverse to the electron beam.

Jefferson Lab can make a unique contribution to studies of the π^+ transverse spin asymmetry via the ability to take measurements at multiple beam energies and unambiguously isolate the longitudinal component of the asymmetry using a Rosenbluth separation. Unfortunately, due to the single beam energy, such a separation was not feasible at HERMES. In comparison to the earlier HERMES measurement, the experiment proposed here will probe higher Q^2 and x, and comparable values of t.

Refs. [3] and [11] also point out that the study of the transverse single-spin asymmetry at low $-t$ is important for the reliable extraction of the pion form factor from electroproduction experiments (Fig. 2b). Investigations of hard exclusive π^+ electroproduction using a pQCD factorization model [14, 15] find that at $x = 0.3$ and $-t = -t_{min}$, the pion pole contributes about 80% of the longitudinal cross section. Since the transverse single-spin asymmetry is an interference between pseudoscalar and pseudovector contributions, its measurement would help constrain the non-pole pseudovector contribution, and so assist the more reliable extraction of the pion form factor. The experimental study of the pion form factor has been approved as an important part of the JLab 12 GeV program [16], and the measurement of the transverse single-spin asymmetry is a logical step in the support of that program.

C. Reasons why a Rosenbluth separation is required

Because transverse photon amplitudes are suppressed by $1/Q$, at very high Q^2 it is safe to assume that all observed meson production is due to longitudinal photons. At the $Q^2 = 2-4$ GeV^2 typical of the Jefferson Lab and HERMES programs, however, this is not the case. Bartl and Majerotto [17] have shown that the transverse single-spin asymmetry in exclusive π^+ electroproduction not only has contributions from the purely longitudinal amplitude discussed in Refs. [3, 8, 9, 11], but also has contributions from transverse-transverse and longitudinal-transverse interference amplitudes.

They express the transversely-polarized nucleon cross section as

$$\frac{d\sigma_\perp}{dt} = \frac{P_y p_\pi W}{KM}[Im\ Y_1 + \epsilon\ \cos 2\phi\ Im Y_2 + 2\epsilon\ Im\ Y_3 + \sqrt{2\epsilon(1+\epsilon)}\ \cos\phi\ Im\ Y_4], \qquad (7)$$

where P_y is the nucleon polarization component parallel to $\hat{q} \times \hat{p_p}$, p_π,p_p are the outoing pion and proton momenta in the virtual photon–nucleon center of mass frame, W is the invariant mass of the hadronic system, $K = (W^2 - M^2)/2M$ is the so–called equivalent photon energy, and

$$Y_1 = h_+^N h_+^{F^*} \; + h_-^N h_-^{F^*} \tag{8}$$

$$Y_2 = h_-^N h_-^{F^*} \; - h_+^N h_+^{F^*} \tag{9}$$

$$Y_3 = h_0^N h_0^{F^*} \tag{10}$$

$$Y_4 = h_0^N h_-^{F^*} \; - h_0^F h_-^{N^*} \tag{11}$$

The h's are helicity amplitudes, where the superscripts F and N indicate baryon spin-flip and non-spin-flip amplitudes, respectively, and the subscripts 0, +, − indicate virtual photon polarizations longitudinal, parallel to the scattering plane, and perpendicular to the scattering plane. Thus, the desired term for study is Y_3, but at HERMES and Jefferson Lab energies one cannot ignore the contributions of Y_1, Y_2 and Y_4 to the observed asymmetry. Y_1 is especially problematic, because it can only be separated from Y_3 with the use of a Rosenbluth separation. The transverse contributions to Y_1 can be estimated using a Regge model [18]. Preliminary indications are that the transverse photon transverse nucleon spin asymmetry is smaller than the longitudinal photon transverse nucleon spin asymmetry, but nonzero for JLab kinematics, and so the experiment must be designed from the beginning to account for this contribution.

Looking more thoroughly at the contributions to the transverse nucleon spin asymmetry in the context of the (slightly modified) notation of Bartl and Majerotto [17], in the case of an unpolarized beam and unpolarized nucleon the virtual photoproduction cross section can be written as

$$\frac{d\sigma}{d\Omega} = \sigma_T + \epsilon \; \sigma_L + \epsilon \; \sigma_{TT} \cos 2\phi + \sqrt{\frac{1}{2}\epsilon(1+\epsilon)} \; \sigma_{LT} \cos\phi, \tag{12}$$

where σ_T, σ_L, σ_{TT}, and σ_{LT} are the usual (modulo some factors of 2) transverse, longitudinal and interference cross sections and ϕ is the azimuthal angle between the reaction plane and the scattering plane. These cross sections can be broken down into helicity amplitudes as follows:

$$\sigma_T = \frac{p_\pi W}{KM}\frac{1}{2}\left(|h_+^N|^2 + |h_+^F|^2 + |h_-^N|^2 + |h_-^F|^2\right) \tag{13}$$

$$\sigma_L = \frac{p_\pi W}{KM}\left(|h_0^N|^2 + |h_0^F|^2\right) \tag{14}$$

$$\sigma_{TT} = \frac{p_\pi W}{KM}\frac{1}{2}\left(|h_-^N|^2 + |h_-^F|^2 - |h_+^N|^2 + |h_+^F|^2\right) \tag{15}$$

$$\sigma_{LT} = \frac{p_\pi W}{KM} 2Re\left(h_0^N h_-^{N^*} + h_0^F h_-^{F^*}\right). \tag{16}$$

For a polarized nucleon, there is an additional contribution to the cross section:

$$\begin{aligned}\sigma_t = P_x &\left[-\sqrt{2\epsilon(1+\epsilon)}\sin\phi\ \sigma_{LT}^x - \epsilon\sin 2\phi\ \sigma_{TT}^x\right] \\ &- P_y\left[\sigma_{TT}^y + \epsilon\cos 2\phi\ \sigma_{TT'}^y + 2\epsilon\ \sigma_L^y + \sqrt{2\epsilon(1+\epsilon)}\cos\phi\ \sigma_{LT}^y\right] \\ &+ P_z\left[\epsilon\sin 2\phi\ \sigma_{TT}^z + \sqrt{2\epsilon(1+\epsilon)}\sin\phi\ \sigma_{LT}^z\right],\end{aligned} \tag{17}$$

where the various cross sections are given by:

$$\sigma_{LT}^x = \tfrac{p_\pi W}{KM} Im\ X_1 \tag{18}$$

$$\sigma_{TT}^x = \tfrac{p_\pi W}{KM} Im\ X_2 \tag{19}$$

$$\sigma_{TT}^y = \tfrac{p_\pi W}{KM} Im\ Y_1 \tag{20}$$

$$\sigma_{TT'}^y = \tfrac{p_\pi W}{KM} Im\ Y_2 \tag{21}$$

$$\sigma_L^y = \tfrac{p_\pi W}{KM} Im\ Y_3 \tag{22}$$

$$\sigma_{LT}^y = \tfrac{p_\pi W}{KM} Im\ Y_4 \tag{23}$$

$$\sigma_{TT}^z = \tfrac{p_\pi W}{KM} Im\ Z_2 \tag{24}$$

$$\sigma_{LT}^z = \tfrac{p_\pi W}{KM} Im\ Z_1\ . \tag{25}$$

The Y amplitudes have been defined earlier, and the X and Z amplitudes are made up of additional linear combinations of helicity amplitudes. The subscripts on each "cross section" denote whether they contain longitudinal amplitudes, transverse amplitudes, or both.

The x, y, and z components of the recoil nucleon polarization are denoted P_x, P_y, and P_z. In the co-ordinate system used here, the z direction is along the virtual photon direction ($\vec{q}$), the y-axis is perpendicular to the hadron reaction plane (in the direction of $\vec{q} \times \vec{p_p}$), and the x direction is given by $\hat{y} \times \hat{z}$.

In this discussion, we are interested in the transverse nucleon spin asymmetries, so we will ignore the terms proportional to P_z. If we define β to be the azimuthal angle between the component of the recoil nucleon polarization perpendicular to $\vec{q}$ ($P_\perp$) and the hadron reaction plane, we can re–express P_x and P_y as:

$$P_x = P_\perp \cos\beta \tag{26}$$

$$P_y = P_\perp \sin\beta \tag{27}$$

Note that if we set all the transverse amplitudes to zero in the above expressions for the unpolarized + polarized cross sections, we are left with

$$\frac{d\sigma}{d\Omega} = \epsilon\,\sigma_L - 2\epsilon\,\sigma_L^y\,P_\perp \sin\beta\,. \tag{28}$$

This is the basis for the exclusive pion transverse nucleon spin asymmetry defined in Ref.[8], which essentially extracts the ratio of σ_L^y to σ_L. For very large values of Q^2, transverse amplitudes should be small, so the above asymmetry can likely be extracted with no explicit L–T separation to isolate the longitudinal components. However, at the kinematics accessible at JLab one cannot assume that this will be the case, so we must take care to address the transverse contributions appropriately.

Experimentally, the angle between the nucleon polarization and the reaction plane, β, and the angle between the scattering and reaction planes, ϕ, are not independent. If the recoil nucleon polarization is at some angle, Φ, relative to the scattering plane, then $\beta = \Phi - \phi$. If we re–express the above cross sections in terms of β and Φ. The polarized nucleon cross section then becomes:

$$\begin{aligned}
\sigma_t = -P_\perp \sin\beta\,[\sigma_{TT}^y + 2\epsilon\,\sigma_L^y] \\
- P_\perp \sin\beta\,[\epsilon(\cos 2\Phi\cos 2\beta + \sin 2\Phi \sin 2\beta)\,\sigma_{TT'}^y] \\
- P_\perp \sin\beta\left[\sqrt{2\epsilon(1+\epsilon)}(\cos\Phi\cos\beta + \sin\Phi\sin\beta)\,\sigma_{LT}^y\right] \\
- P_\perp \cos\beta\left[\sqrt{2\epsilon(1+\epsilon)}(\sin\Phi\sin\beta - \cos\Phi\cos\beta)\,\sigma_{LT}^x\right] \\
- P_\perp \cos\beta\,[\epsilon(\sin 2\Phi\sin 2\beta - \cos 2\Phi\cos 2\beta)\,\sigma_{TT}^x]\,.
\end{aligned} \tag{29}$$

From the above equation, it is clear that to extract the (longitudinal photon) transverse nucleon spin asymmetry it is necessary to first isolate the $\sin\beta$ Fourier component of the polarized nucleon cross section. Once that has been accomplished, one must then separate the σ_L^y term from the σ_{TT}^y term via a Rosenbluth-type separation. This is what we propose to do in this experiment.

III. EXPERIMENTAL METHOD

A. Set–up and Kinematics

We intend to pursue this measurement in Hall C, using the HMS in coincidence with the SHMS. While exclusive pion production measurements using CLAS-12 and a transversely polarized ^{1}H target have been discussed previously [19], measurements utilizing the HMS–SHMS over a more limited kinematic range can be of great value because they allow the systematic error control necessary to perform a high quality Rosenbluth separation. Thus, we can demonstrate whether the dominance of the longitudinal contribution to the single spin asymmetry at intermediate Q^2 is in fact a valid assumption.

^{2}H will be used to provide a neutron target in quasi-free kinematics for the reaction. The recoil proton polarization will be measured by the hadron arm FPP to be commissioned for the 12 GeV G_{ep}/G_{mp} experiment. The experiment kinematics are such that either the HMS or SHMS could be used to detect the recoil proton, depending on where the FPP is installed at the time. Thus, the reaction of interest is $d(e, e'\vec{p})\pi^- p_{sp}$. The measurement of the transverse single-spin asymmetry requires the detection of the recoil proton in non-parallel kinematics. It is the component of the proton polarization parallel to $\hat{q} \times \hat{p_\pi}$ that is important (Eqn. 7), and this direction is uniquely defined only in non-parallel kinematics.

The choice of the recoil polarization technique is dictated by the luminosity required to perform this measurement in a reasonable amount of time. An unpolarized ^{2}H target allows the full 100 μA beam current to be used. The use of the UVa polarized NH_3 target in the $\vec{p}(e, e'\pi^+)n$ reaction was also investigated, but the maximum beam current that can then be used is only 85 nA and the running times are lengthened accordingly.

The recoil polarization technique comes with its own complications, however. Kinematics must be found where the recoil proton has sufficient momentum to allow its polarization to be detected with reasonable efficiency. Fig. 5 shows scattering efficiencies as calculated for the Hall A FPP. It is clear that measurements with recoil momenta much below 600 MeV/c are precluded by low scattering efficiencies. This places a lower limit on the Q^2 value and an upper limit on the W value for the experiment. The kinematics which we are considering (see Table I) meet this requirement, and would allow 5.7 cm ($Q^2 = 3.1$ GeV^2) and 7.6 cm ($Q^2 = 4.0$ GeV^2) analyzer thicknesses to be used.

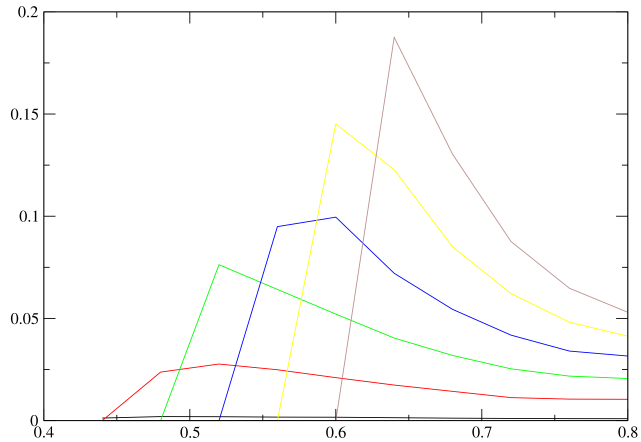

FIG. 5: Scattering efficiency as calculated for the Hall A FPP, as a function of proton momentum (in GeV/c). The six curves correspond to analyzer thicknesses of: 9.5 cm (brown), 7.6 cm (yellow), 5.7 cm (blue), 3.8 cm (green), 1.9 cm (red), and just the 0.5 cm S2 scintillator layer (black). The curves are for a carbon analyzer, but CH_2 will be similar. For the purposes of this LOI, we have assumed the same scattering efficiencies for the Hall C FPP. [Figure courtesy of Ed Brash.]

TABLE I: Near-parallel kinematic settings that we are considering for this experiment. The experiment kinematics are such that either the HMS or SHMS could be used to detect the recoil proton, depending on where the FPP is installed at the time. The linac gradient key is: A: 2.15 GeV/pass "12.0"; B: 1.80 GeV/pass "10.0".

$n(e,e'p)\pi^-$ Kinematic Settings								
E_e (Pass #) (GeV)	$E_{e'}$ (GeV)	$\theta_{e'}$ (deg)	ϵ	θ_q (deg)	p_π (GeV/c)	θ_π (deg)	p_p (GeV/c)	θ_p (deg)
$Q^2 = 3.10$ GeV^2, $W = 2.10$ GeV								
5.50 (3B)	1.973	30.99	0.565	-14.94	3.359	-14.94	0.584	-14.94
9.10 (5B)	5.573	14.20	0.865	-20.30	3.359	-20.30	0.584	-20.30
$Q^2 = 4.00$ GeV^2, $W = 2.30$ GeV								
6.60 (3A)	2.126	30.96	0.521	-12.90	4.263	-12.90	0.609	-12.90
10.90 (5A)	6.426	13.72	0.852	-18.13	4.263	-18.13	0.609	-18.13

After a second scattering in the hadron arm analyzer, the modulation of the ${}^{12}C(\vec{p},p')$ cross section with the azimuthal angle, Φ_s, around the polarization independent part,

$\sigma_p(\Theta_s, T_p)$,

$$\sigma = \sigma_0(\Theta_x, T_p)[1 + A_c(\Theta_s, T_p)(P_y^{fp} cos\Phi_s - P_x^{fp} sin\Phi_s)], \tag{30}$$

is measured by the FPP. This allows the extraction of the two polarization components perpendicular to the proton momentum, P_x^{fp} and P_y^{fp} (fp indicates focal plane).

To connect these polarization components to those at the target, the proton's spin precession through the spectrometer magnetic elements must be taken into account. This is described by a rotation of the initial spin, given in the spectrometer-target frame (tg), into the final direction, expressed in the particle frame (fp), which is fixed to the particle direction behind the focal plane. It can be written in matrix form:

$$\begin{pmatrix} S_x \\ S_y \\ S_z \end{pmatrix}^{fp} = \begin{pmatrix} M_{xx} & M_{xy} & M_{xz} \\ M_{yx} & M_{yy} & M_{yz} \\ M_{zx} & M_{zy} & M_{zz} \end{pmatrix} \begin{pmatrix} S_x \\ S_y \\ S_z \end{pmatrix}^{tg} . \tag{31}$$

Restricting Eqn. 31 to the two measurable focal plane polarization components and replacing the spins by the polarizations, the polarization components in the electron scattering plane can be obtained:

$$\begin{pmatrix} P_x \\ P_y \end{pmatrix}^{fp} = \begin{pmatrix} M_{xx} & M_{xy} & M_{xz} \\ M_{yx} & M_{yy} & M_{yz} \end{pmatrix} \cdot T_{\alpha\beta} \cdot \begin{pmatrix} P_x \\ P_y \\ P_z \end{pmatrix}^{sp} . \tag{32}$$

The M_{ij} are the elements of the spectrometer's spin transfer matrix (STM) and $T_{\alpha\beta}$ is the 3×3 kinematic matrix describing the rotation between the spectrometer-target and scattering-plane coordinate frames. For a homogeneous dipole field, $M_{xx} = 1$, $M_{xy} = M_{xz} = 0$ and M_{yz} =sinχ_0, where χ_0 is the dipole bend angle. The effect of the SHMS horizontal bender, quadrupoles, fringe fields, and the radial field gradient in the dipole alter the STM from this simple picture. We expect to work closely with the G_{ep}/G_{mp} collaboration to ensure that these elements are known to the required level of precision.

Finally, the angle β between the recoil polarization and the reaction plane will be computed for each $(Q^2, W, -t, \epsilon, \phi_{pq})$ bin and the σ_L and σ_L^y terms determined in a Rosenbluth-type separation.

B. Simulation of the Experiment - Acceptance

Preliminary simulations of this proposed measurement have been carried out using the standard Hall C Monte Carlo, SIMC. For these simulations, we have assumed that the scattered electron is detected in the HMS, and the recoil proton in the SHMS. The simulations include radiative effects, effects from multiple scattering, and a pion electroproduction cross section model. In this case, the pion cross section used was a parameterization consistent with the separated cross sections extracted in the two pion form–factor experiments, E93-021 and E01-004 [20].

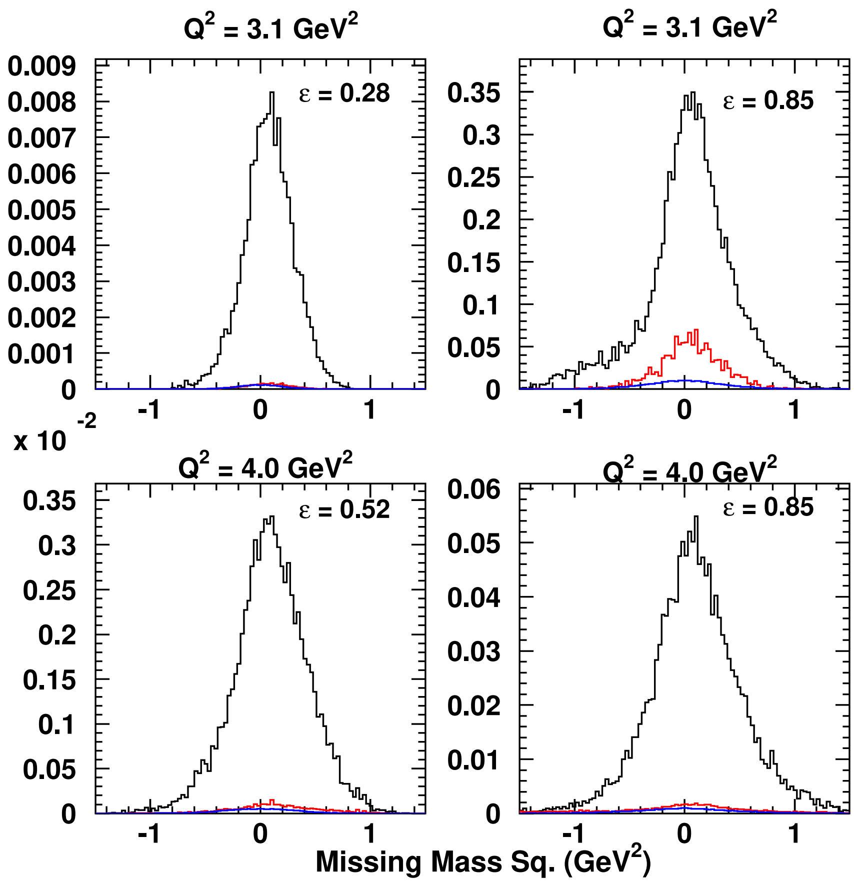

FIG. 6: Simulated missing mass squared distributions for the ^{2}H$(e, e'p)\pi^- p$ reaction (black), ^{2}H$(e, e'p)\pi^0 n$ (red) and ^{2}H$(e, e'p)\gamma n$ (blue). The π^0 distributions are scaled upwards by factors of 5 at $Q^2 = 3.1$ GeV^2 and 20 at $Q^2 = 4.0$ GeV^2 in order to make them visible. Similarly, the hard photon distributions are scaled upwards by factors of 2000 at $Q^2 = 3.1$ GeV^2 and 200 at $Q^2 = 4.0$ GeV^2. Thus, these background contributions are expected to be very small.

One of the first considerations is the ability to distinguish the exclusive final state. Fig. 6 shows the simulated missing mass spectra for both of the ϵ settings at $Q^2 = 3.1$ and 4.0 GeV^2. One of the drawbacks of the recoil detection technique is unfortunately that the missing mass resolution suffers in comparison to if the π was detected.

With the use of the ^{2}H target and recoil detection, there are several sources of background which must be taken into account. Two of these are π^0 production via $d(e, e'\vec{p})\pi^0 n_{sp}$, and hard photon production via the Bethe-Heitler and DVCS processes, $d(e, e'\vec{p})\gamma n_{sp}$. Their simulated contributions to the missing mass distribution are also shown in Fig. 6. The hard photon simulation is normalized according to the DVCS+Bethe-Heitler model used by the HERMES Collaboration [21]. The π^0 simulations use the Regge model by Vanderhaeghen, Guidal and Laget [18], which acceptably describes the existing π^0 data. Thus, these studies indicate that these background processes are expected to have negligible contributions.

Preliminary simulations of the 2π production process have also been performed, and a missing mass distribution with *arbitrary normalization* is shown in Fig. 7. One might expect these contributions to be suppressed by the high values of z chosen for this experiment,

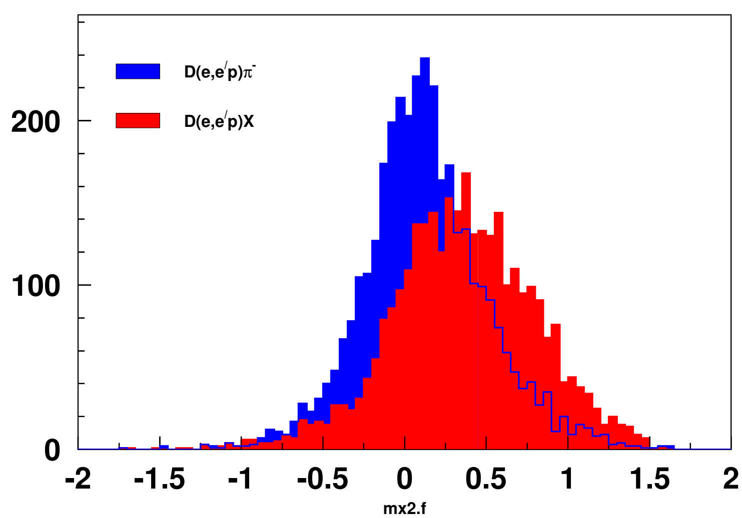

FIG. 7: Simulated missing mass squared distribution for the background process ^{2}H$(e, e'p)2\pi X$ (red) and the foreground process ^{2}H$(e, e'p)\pi^- n_{sp}$ (blue). The 2π distribution is arbitrarily normalized; further investigations are required before submitting a full proposal

and further investigations are required before submitting a full proposal. We intend to substantially reduce these contributions by application of a missing mass cut, and in addition by repeating the experiment on a ^{1}H target and, after smearing with the ^{2}H spectral function, subtracting from each bin the measured yields which survive the cuts prior to doing the separation. The contributions of other sources of background, such as $p(e, e'\vec{n})\pi^+$ followed by $p(\vec{n}, \vec{p})n$ are still under investigation.

Ideally, one would like full coverage of the angle between the recoil proton polarization vector and the reaction plane, β over the full range of t. The expected coverage for this experiment is shown in Fig. 8. No $\sin\beta$ term was used to generate this distribution, hence the large numbers of simulated events in the vicinity of $\pi/2$ and $3\pi/2$ are due to the acceptance

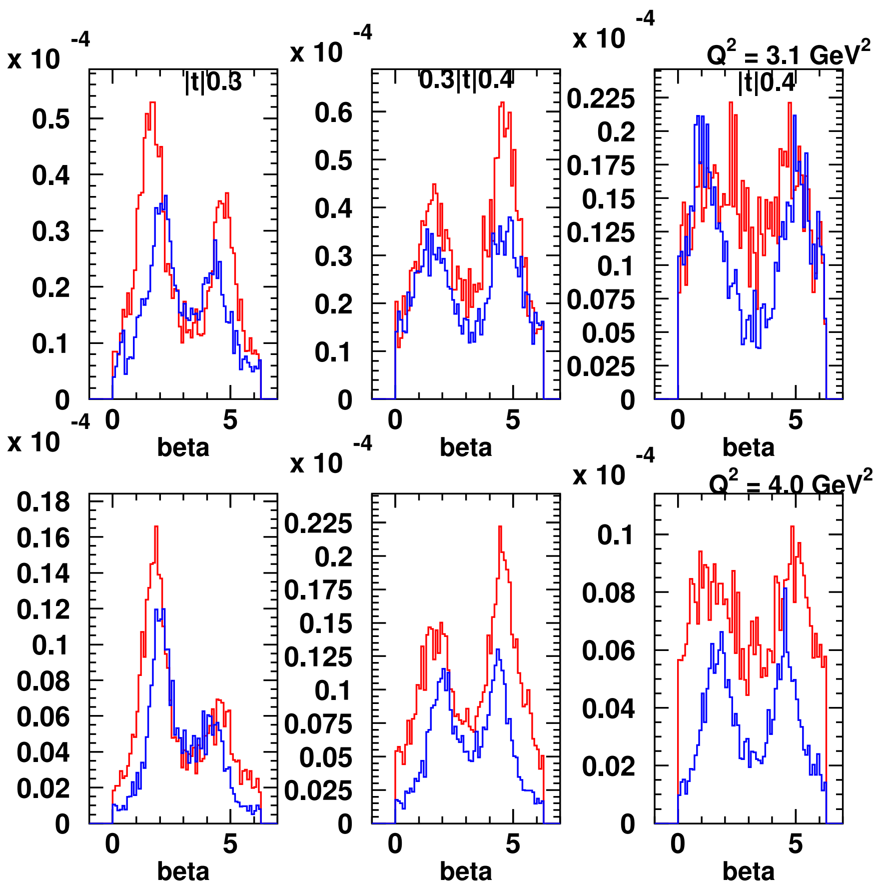

FIG. 8: Simulated distributions of the azimuthal angle of the recoil proton polarization with respect to the hadron reaction plane, β, for three t bins spanning the kinematic range of the data. The blue curves are the large ϵ distributions and red curves are small ϵ. These figures indicate full coverage in β at high and low ϵ across the t range sampled by the experiment.

of the experimental configuration. This type of β coverage is well-suited to extracting the $\sin\beta$ term of the polarized cross section given in Eqn. 29.

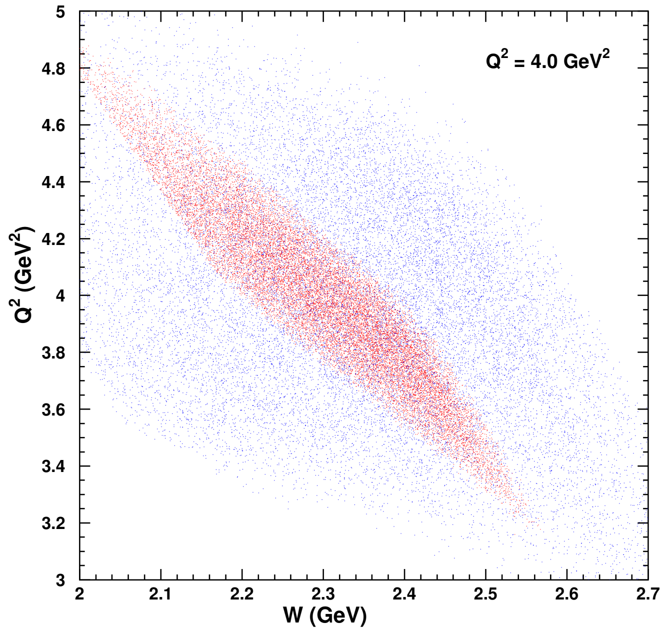

FIG. 9: Simulated experimental acceptance in Q^2 and W for the high (blue) and low (red) ϵ settings at $Q^2 = 4.0$ GeV^2. A "diamond" cut will be applied to match the kinematic coverages of the low and high ϵ data.

While the kinematics in Table I are for the nominal central values of Q^2 and W (or x_B), the experimental acceptance allows a range of x_B, Q^2 and t to be sampled. This is desirable because the transverse spin asymmetry vanishes at $-t_{min}$ (parallel kinematics) and grows rapidly as $-t$ is increased. The kinematic coverage of the experiment is illustrated in Figs. 9 and 10. The coverage is sufficiently large to allow the data at each Q^2 to be broken into three t–bins.

C. Rates and Estimate of Uncertainties

The SIMC simulations used for the above acceptance studies incorporate a cross section model [20] whose normalization has been checked against the available data. Thus, they can be used to reliably extract rate estimates. In preparing the estimates, we assume the use of 10 cm cryogenic targets and 100 μA beam currents. Upon application of reasonable acceptance cuts and the phase-space matching cuts necessary for the L-T separation (Fig. 9),

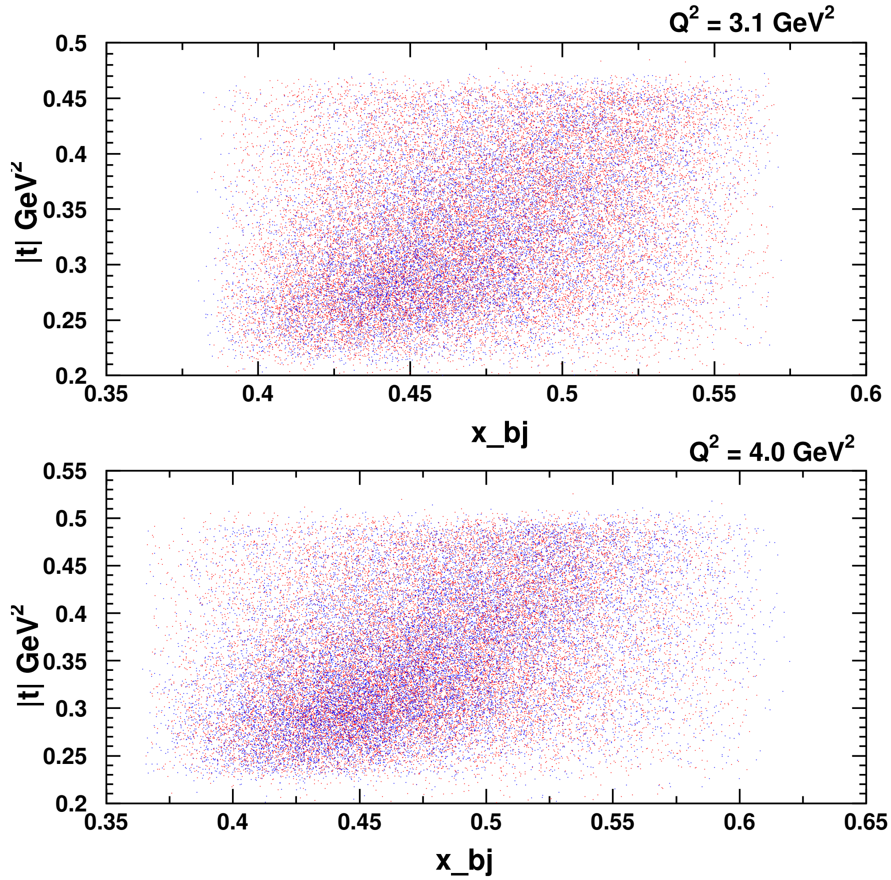

FIG. 10: Simulated experimental acceptances in $-t$ and x_B for the high (blue) and low (red) ϵ settings. Cuts in Q^2 and W have already been implemented to match the kinematic coverages of the low and high ϵ data.

we estimate real coincidence rates of 297(72) per hour for the $Q^2 = 3.1$ GeV^2, $\epsilon = 0.87(0.57)$ settings, and real coincidence rates of 137(38) per hour for the $Q^2 = 4.0$ GeV^2, $\epsilon = 0.85(0.53)$ settings.

The statistical uncertainties in the focal plane polarization components in Eqn. 30 are given by

$$dP_i^{fp} = \sqrt{\frac{2}{N_0 \epsilon_{FPP} A_y^2}} \tag{33}$$

where N_0 is the number of valid coincidences in a given t-bin after all cuts, ϵ_{FPP} is the second scattering efficiency, and A_y is the mean analyzing power. These statistical uncertainties are magnified if the spin precession through the spectrometer magnetic elements is unfavorable. For the recoil proton momenta proposed here, the spin precession in the SHMS is approximately 42^o and results in a very small additional uncertainty in the measured recoil polarization.

Our uncertainty estimates assume mean efficiencies of $\epsilon_{FPP} = 0.085(0.12)$ at $Q^2 = 3.1(4.0)$ GeV^2, based on the 5.7 and 7.6 cm analyzer curves in Fig. 5. Recent Hall A data [22] also indicate a mean analyzing power of approximately $A_y = 0.40$ for $7^o - 25^o$ second scattering angles. At ~ 600 MeV/c, the Coulomb scattering peak extends to larger angles than at higher momenta, so the lower cutoff is taken as 7^o rather than 5^o. However, the region with useful A_y also extends to higher angles and so second scatterings up to 25^o can be used, rather than the 20^o typically used at higher momenta.

Assuming running times of 310(430) hours for the $Q^2 = 3.1$ GeV^2, $\epsilon = 0.87(0.57)$ settings, we expect to measure the recoil polarization components with an uncertainty of $dP_i^{fp} = 0.07$ *per t bin* at high ϵ and $dP_i^{fp} = 0.12$ at low ϵ. At $Q^2 = 4.0$ GeV^2, running times of 475(570) hours are required to achieve the same polarization uncertainties. Although the coincidence rate at $Q^2 = 3.1$ GeV^2 is expected to be higher than at $Q^2 = 4.0$ GeV^2, this is offset somewhat by the relatively lower FPP efficiency. The two Q^2 settings thus take similar amounts of beamtime, and both are presented here to indicate two options which can be pursued further in the full proposal.

MY MODIFICATIONS STOP HERE. DAVE CAN YOU PLEASE FINISH THE REST?

The quantity we ultimately wish to extract is a ratio of two longitudinal cross sections. As typically defined (i.e. Eqn. 6), the transverse nucleon spin asymmetry as written in our notation corresponds to,

$$A_\perp = \frac{1}{P_\perp}\frac{2}{\pi}\frac{2\sigma_L^y}{\sigma_L} \ , \tag{34}$$

where σ_L^y and σ_L were defined earlier in Sec I-C. To obtain a rough estimate of the expected uncertainty in such a measurement, we assume the polarized recoil cross section has the following simplified form,

$$\sigma = \sigma_T + \epsilon\sigma_L - P_\perp \sin\beta \left(\sigma_T^y + \epsilon 2\sigma_L^y\right) \ . \tag{35}$$

The final uncertainty in any L–T separated cross section is sensitive to the ratio of the longitudinal to transverse cross sections ($R = \frac{\sigma_L}{\sigma_T}$). For the calculations here, we assume an average value of ...

The polarized longitudinal cross section is in general less well studied, so for now we assume the longitudinal response is the same size as the transverse ($\sigma_L^y = \sigma_T^y$). We then used the Monte Carlo to simulate the relative $-t$ distribution of events for each ϵ setting, and

$-t$	$\langle x_B \rangle$	Counts	$\frac{\delta\sigma}{\sigma}_{stat}(\%)$	$\frac{\delta\sigma_L}{\sigma_L}(\%)$	$\frac{\delta\sigma^y}{\sigma^y}_{stat}(\%)$	$\frac{\delta\sigma^y_L}{\sigma^y_L}(\%)$
$Q^2 = 3.1$ GeV^2						
<0.30	0.43	1830	1.0	20.8	4.7	31.2
0.30–0.40	0.48	33000	0.8	20.6	3.8	27.9
>0.40	0.52	8940	1.1	20.9	4.8	31.5
$Q^2 = 4.0$ GeV^2						
<0.30	0.43	10650	1.0	20.8	4.7	31.2
0.30–0.40	0.47	14900	0.8	20.6	3.8	27.9
>0.40	0.53	8940	1.1	20.9	4.8	31.5

TABLE II: Projected statistical errors on the unseparated cross sections in each $-t$–bin assuming the running times listed in the text. Also shown is the total uncorrelated error on the longitudinal cross sections assuming 4% point–to–point systematic errors. The above calculations assume that the asymmetry (or longitudinal ratio) as defined in Eqn. 34 is 0.3. Note that if the asymmetry is significantly larger, the statistical precision on the σ^y_L improves for the same number of counts. NOTE, ALL OF THESE NUMBERS ARE WRONG!

determined the statistical uncertainty in fitting the constant $(\sigma_T + \epsilon\sigma_L)$ and $\sin\beta$ $(\sigma^y_T + \epsilon\sigma^y_L)$ terms of the unseparated cross sections.

As with any L–T separation, the uncertainty in the longitudinal piece is subject to the usual $1/\Delta\epsilon$ amplification. This means that we are the most sensitive to uncertainties that propagate randomly between ϵ settings. There is a lot of experience in Hall C with L–T separations and their uncertainties. For the HMS–SOS set–up, it is typically assumed that uncorrelated errors in meson electroproduction experiments can be controlled to the 2–2.5% level. For the SHMS–HMS, the uncorrelated errors are expected to be similar.

An example of the projected statistical and total uncorrelated error for each $-t$–bin is shown in Table II. In the end, we need to take the ratio of cross sections to obtain the asymmetry, and in taking that ratio, some of the systematic errors that are typically uncorrelated when one one determines an *absolute* separated cross section become partially correlated when one takes the ratio of separated cross sections. In the present estimates, we ignore these partially correlated errors, and treat all errors that are uncorrelated in the L–T separations as uncorrelated in the separated ratios as well.

PROJECTED ERROR BARS PLOT GOES HERE.

FIG. 11: Projected uncertainties for the L–T *separated* transverse nucleon spin asymmetry, assuming $A_\perp = 0.2$ (red circles) and $A_\perp = 0.5$ (blue squares). Curves are predictions at various vaules of $-t$ from Ref. [11]. Each projected x_B point corresponds to the $-t$ range noted in Table II.

Finally, the projected uncertainties for the transverse single spin asymmetry are shown in Fig. 11. The uncertainties on these points ignore correlated uncertainties that should mostly cancel in the ratio. Assuming we can achieve 2-3% precision on this quantity, it is a minimal contribution to the uncertainty on the separated ratios. It is also worth mentioning that the unseparated ratio can be measured with very good precision (on the order of 5–10% relative) since the uncorrelated errors for σ_L^y and σ_L are still rather small when combined in quadrature at a particular ϵ.

D. Further Studies

Before submitting a full proposal, there are of course several more studies that we would like to make.

---

[1] M. Diehl, arXiv:hep-ph/0010200.

[2] J.C. Collins, L. Frankfurt, M. Strikman, Phys. Rev. D **56** (1997) 2982.

[3] K. Goeke, M.V. Polyakov, M. Vanderhaeghen, Prog. Part. Nucl. Phys. **47** (2001) 401-515.

[4] A.V. Radyushkin, arXiv:hep-ph/0101225.

[5] A.W. Thomas, W. Weise, "The Structure of the Nucleon", J. Wiley-VCH, 2001.

[6] R.E. Marshak, Riazuddin, C.P. Ryan, "Theory of Weak Interactions in Particle Physics", J. Wiley, 1969.

[7] M. Penttinen, M.V. Polyakov, K. Goeke, Phys. Rev. C **62** (2000) 014024 1-11.

[8] A.V. Belitsky, D. Mueller, Phys. Lett. **B 513** (2001) 349-360.

[9] L.L. Frankfurt, P.V. Pobylitsa, M.V. Polyakov, M. Strikman, Phys. Rev. D **60** (1999) 014010 1-11.

[10] M. Vanderhaeghen, P.A.M. Guichon, M. Guidal, Phys. Rev. D **60** (1999) 094017 1-28.

[11] L.L. Frankfurt, M.V. Polyakov, M. Strikman, M. Vanderhaeghen, Phys. Rev. Lett. **84** (2000) 2589-2592.

[12] A.V. Belitsky, CIPANP 2003 proceedings. arXiv: hep-ph/0307256.

[13] A. Airapetian, et al., Phys. Lett. **B 535** (2002) 85-92.

[14] L. Mankiewicz, G. Piller, A. Radyushkin, Eur. Phys. J. **C 10** (1999) 307-312.

[15] C.E. Carlson, J. Milana, Phys. Rev. Lett. **65** (1990) 1717.

[16] E12-06-101, "Measurement of the Charged Pion Form Factor to High Q^2", G.M. Huber, D. Gaskell, spokespersons.

[17] A. Bartl, W. Majerotto, Nucl. Phys. **B62** (1973) 267-285.

[18] M. Vanderhaeghen, M. Guidal, J.-M. Laget, Phys. Rev. C **57** (1998) 1454.

[19] pCDR for the Science and Experimental Equipment for the 12 GeV Upgrade of CEBAF, June, 2004.

V. Burkert et al., PAC18 Review of the Science Driving the 12 GeV Upgrade, July, 2000.

[20] T. Horn, parameterization of $p(e, e'\pi^+)n$ separated cross sections, 2006.

[21] Subroutine gen_bhdvcs, written by V. Korotkov.

[22] J. Glister, E05-103 Status Report, January 4, 2007, and A. Sarty, private communication.